Published in final edited form as:
J Mech Behav Biomed Mater. 2009 August ; 2(4): 339–347. doi:10.1016/j.jmbbm.2008.10.005.

NANOINDENTATION OF THE INSERTIONAL ZONES OF HUMAN MENISCAL ATTACHMENTS INTO UNDERLYING BONE

K.N. Hauch[1], **M.L. Oyen**[2], **G.M. Odegard**[1], and **T. L. Haut Donahue**[1]

[1] Department of Mechanical Engineering, Michigan Technological University, Houghton, MI 49931, USA

[2] Cambridge University Engineering Department, Cambridge, CB2 1PZ, UK

Abstract

The fibrocartilagenous knee menisci are situated between the femoral condyles and tibia plateau and are primarily anchored to the tibia by means of four attachments at the anterior and posterior horns. Strong fixation of meniscal attachments to the tibial plateau provide resistance to extruding forces of the meniscal body, allowing the menisci to assist in load transmission from the femur to the tibia. Clinically, tears and ruptures of the meniscal attachments and insertion to bone are rare. While it has been suggested that the success of a meniscal replacement is dependent on several factors, one of which is the secure fixation and firm attachment of the replacement to the tibial plateau, little is known about the material properties of meniscal attachments and the transition in material properties from the meniscus to subchondral bone. The objective of this study was to use nanoindentation to investigate the transition from meniscal attachment into underlying subchondral bone through uncalcified and calcified fibrocartilage. Nanoindentation tests were performed on both the anterior and posterior meniscal insertions to measure the instantaneous elastic modulus and elastic modulus at infinite time. The elastic moduli were found to increase in a bi-linear fashion from the external ligamentous attachment to the subchondral bone. The elastic moduli for the anterior attachments were consistently larger than those for the matching posterior attachments at similar indentation locations. These results show that there is a gradient of stiffness from the superficial zones of the insertion close to the ligamentous attachment into the deeper zones of the bone. This information will be useful in the continued development of successful meniscal replacements and understanding of fixation of the replacements to the tibial plateau.

Keywords

Nanoindentation; meniscus; enthesis; material properties; knee

INTRODUCTION

Previous computational and experimental studies have shown that the attachments of the menisci at the anterior and posterior horns are important for the menisci to distribute load in the knee (Chen, Branch et al. 1996; Goertzen, Gillquist et al. 1996; Messner and Gao 1998;

Corresponding Author: Tammy Haut Donahue, Department of Mechanical Engineering, 1400 Townsend Dr., Houghton, MI 49931, E-mail: thdonahu@mtu.edu, 001 906 487 2078.

Alhalki, Howell et al. 1999; Setton, Guilak et al. 1999; Cole, Carter et al. 2002). Meniscal horn attachments anchor the menisci to the underlying subchondral bone. Successful meniscal replacements must restore the horn attachments of the menisci (Setton, Guilak et al. 1999), hence recent studies have been aimed at characterizing the material properties of the ligamentous horn attachments (Maes and Haut Donahue 2006; Villegas, Maes et al. 2007).

Meniscal attachments can be considered as having two parts; the external ligamentous portion and the insertional area consisting of different zones. The insertional zones have been characterized as: ligamentous, uncalcified fibrocartilage, calcified fibrocartilage, and subchondral bone, and have been found at meniscal attachment insertions as well as at ligament-bone interfaces (Cooper and Misol 1970; Benjamin, Evans et al. 1991; Gao, Oqvist et al. 1994; Gao, Rasanen et al. 1996; Gao 2000; Villegas, Hansen et al. 2008). Meniscal attachment ruptures *in vivo* are rare, therefore the insertional zones likely aid in transitioning from the external ligamentous attachment to the underlying subchondral bone, reducing large stress concentrations at the bone interface. The thickness of the uncalcified and calcified fibrocartilage zones have been found to be on the order of 0.1–0.4 mm (Benjamin, Evans et al. 1991) and have been studied in both human (Benjamin, Evans et al. 1991) and bovine (Villegas, Hansen et al. 2008) subjects. The thickness of the zones and the microstructure of the interfaces between the zones does not allow separation of the zones for mechanical testing.

Nanoindentation in the biomechanics field has been used to determine: the elastic modulus and hardness of human bone (Rho, Roy et al. 1999; Hengsberger, Kulik et al. 2001; Ferguson, Bushby et al. 2003; Bushby, Ferguson et al. 2004) and articular calcified cartilage (Ferguson, Bushby et al. 2003), as well as the viscoelastic properties of fibrocartilage and bone (Hu, Radhakrishnan et al. 2001) (Bembey,Bushby et al. 2006). Nanoindentation has more recently been used to correlate mechanical behavior with mineralization (Gupta, Schratter et al. 2005; Oyen 2006). Some advantages of nanoindentation are that it provides high resolution (Rho and Pharr 1999; Rho, Roy et al. 1999; Hoffler, Guo et al. 2005; Tai, Qi et al. 2005), it allows for examination of properties in different directions (Rho, Roy et al. 1999), including characterization of bone anisotropy (Swadener, Rho et al. 2001) and it can be used to characterize the complicated local mechanical properties of heterogeneous materials (Constantinides, Ravi Chandran et al. 2006; Oyen and Ko 2008), which makes it advantageous for application in biological tissues (Ebenstein and Pruitt 2004; Oyen 2006).

There are different probe tip geometries used in nanoindentation, including both sharp (i.e. Berkovich) and blunt (i.e. spherical) shapes suited for measurements of different aspects of the mechanical response. Sharp tips are often used with elastic-plastic analytical models (Oliver and Pharr 1992) for studies of dehydrated, highly mineralized tissues such as bone and calcified cartilage (Rho and Pharr 1999; Ferguson, Bushby et al. 2003). However, in the current study a transition region with an expected wide range of material properties was of interest, and thus a spherical tip geometry was employed. For a large spherical probe, the deformation is dominantly elastic, or in the case of biological materials, viscoelastic (Oyen 2005; Oyen 2007) and analysis appropriate to time-dependent deformation modes is required. Fortunately such analyses are available in the literature (although not built into commercial nanoindentation software) and available for routine use in characterization of biological materials by nanoindentation (Bembey, Bushby et al. 2006).

While the material properties of the insertional zones have not been studied, collagen distribution (Gao 2000) and glycosaminoglycan (GAG) fraction (Villegas, Hansen et al. 2008) within the zones have been previously characterized. Knowledge of the biomechanical characteristics of the zones may help in understanding how these zones assist in the strong fixation of the attachments to the tibial plateau and transition from the meniscus to subchondral bone. In the present study, nanoindentation was used to characterize the gradient of material

properties from the meniscal attachments into the subchondral bone through the uncalcified and calcified fibrocartilage.

MATERIALS AND METHODS

Sample preparation

Three male human knee joints, showing no sign of joint degeneration, were obtained from a national tissue bank (NDRI, Philadelphia, PA) (ages 51–60). Bone blocks around the anterior and posterior meniscal attachments were excised from each knee. The bone blocks were cut such that the inner and outer sides were parallel to the external ligamentous attachment fiber orientation (Figure 1). The bone blocks were then embedded in Struers acrylic cold mounting resin (Citofix powder and Citofix/Durofix-2 liquid, Struers, Cleveland, OH). The bone blocks were not dehydrated prior to embedding. The block was bisected using a low-speed diamond saw (Buehler Isomet 1000, Buehler, Lake Bluff, IL) running at 225 rpm with continuous water irrigation, in order to expose the middle face of the embedded bone block (Figure 1). Surface preparation consisted of using metallographic polishing wheels running at 200 rpm. The sample was ground with progressive grades of silicon carbide paper (600 and 1200 grit) using distilled water as a lubricant and then polished on microcloths with successively finer grades of alumina powder slurries (1 and 0.05 μm grit) (Rho, Roy et al. 1999;Hengsberger, Kulik et al. 2001;Hoffler, Guo et al. 2005;Tai, Qi et al. 2005;Donnelly, Baker et al. 2006). Samples were rinsed with distilled water and were placed in an ultrasonic bath of distilled water between polishing intervals and after all surface preparation was completed in order to remove surface debris (Rho and Pharr 1999;Rho, Roy et al. 1999;Hoffler, Guo et al. 2005;Tai, Qi et al. 2005;Wang, Chen et al. 2006). Embedded samples were wrapped in gauze saturated with 0.9% saline solution and stored at 4°C until time of testing.

Nanoindentation

Test Setup—Nanoindentation experiments were performed on an MTS Nano Indenter XP (MTS Systems, Eden Prairie, MN) using a 300 μm diameter spherical alumina tip (MTS Nano Instruments, Oak Ridge, TN). Each sample was placed in a tray and secured with a set screw so that the polished surface was level with the leveling arms of the tray housed on the x-y stage of the nanoindenter. The attachment insertion region of the bone block was positioned beneath the fixed location of the indenter using the x-y stage. Indentations were made perpendicular to the polished face of the bone block at varying depths from the tibial plateau surface (superficial) into the underlying bone (deep). Several studies have identified three transitional zones at the posterior insertion and four transitional zones present at the anterior insertion of the meniscal attachments into the underlying bone (Gao, Oqvist et al. 1994; Gao 2000; Villegas, Hansen et al. 2008). The four zones are classified as: ligamentous (LI), uncalcified fibrocartilage (UF), calcified fibrocartilage (CF), and subchondral bone (SB) (Figure 1). Individual indentations were separated by 0.05–0.07 mm in the superficial-deep direction (y) (Figure 1). Two parallel columns of indentations were performed with 6 indents in each column. The tidemark between the calcified and uncalcified zones was visible in the images under the nanoindenter microscope, and was treated as a common reference between different samples. The interdigitations between calcified fibrocartilage and subchondral bone were not visible using the optical microscope on the nanoindentor for the thick samples used for nanoindentation, hence it is not possible to separate indents between these 2 zones. It was expected that approximately 2 indents were occurring in each zone.

Indentation Testing and Analysis—Load-controlled creep experiments were performed using a trapezoidal loading sequence (Figure 2a). During the peak load hold segment ($t_{rise} \leq t \leq t_{rise}+t_{hold}$), the specimen creeps under constant load, and therefore the displacement of the indenter tip into the surface increases (Figure 2b). Each nanoindentation test was conducted to

a maximum load (P_{max}) of either 8 or 10 mN, to remain in a small-strain regime based on the indentation depths encountered and tip diameter (Oyen 2007), and with a rise time (t_{rise}) of 20 s, and a hold time (t_{hold}) of 80 s.

The experimental displacement-time data obtained during the creep response ($t_{rise} \leq t \leq t_{rise}+t_{hold}$) was analyzed to obtain the instantaneous shear modulus and shear modulus at infinite time based on viscoelastic analysis of Oyen (Oyen 2005; Oyen 2007) after Lee and Radok (1960) (also summarized by Johnson, 1985) which assumes a constant Poisson's ratio (initially set to 0.5 for incompressible responses) and isotropy(Lee and Radok 1960; Johnson 1985). For a creep function of the form

$$J(t)=C_0 - C_1\exp(-t/\tau_1) - C_2\exp(-t/\tau_2) \tag{1}$$

the displacement-time indentation creep response is of the form

$$h^{3/2}(t)=B_0 - B_1\exp(-t/\tau_1) - B_2\exp(-t/\tau_2) \tag{2}$$

which can be fit using non-linear curve fitting capabilities of Origin (OriginLab, Northampton, MA). The parameters (B_0, B_1, B_2, τ_1, τ_2) obtained from the non-linear curve fitting were used to determine the creep compliance coefficients (C_0, C_1, C_2) via the previously established solutions (Oyen 2005; Oyen 2007)

$$C_0=\frac{B_0}{P_{max}F_G} \tag{3}$$

$$C_{1,2}=\frac{B_{1,2}}{P_{max}F_G RCF_{1,2}} \tag{4}$$

where the ramp correction factor (*RCF*) which accounts for the difference between a step-load (e.g. a Heaviside step function) and a ramp-load creep response is

$$RCF_{1,2}=\frac{\tau_{1,2}}{t_{rise}}(\exp(t_{rise}/\tau_{1,2}) - 1) \tag{5}$$

and the tip geometrical factor is

$$F_G=\frac{3}{8\sqrt{R}} \tag{6}$$

where R is the spherical indenter tip radius. The limiting values of the creep function give the instantaneous shear modulus (G_0) and the shear modulus at infinite time (G_∞) also termed the equilibrium modulus, which were computed from creep compliance coefficients (Oyen 2005; Oyen 2007);

$$G_0=\frac{1}{2(C_0 - C_1 - C_2)} \tag{7}$$

$$G_\infty = \frac{1}{2C_0} \tag{8}$$

The ratio of these modulus values, G_∞/G_0, gives a measure of the importance of time-dependent deformation during the duration of the experiment, with a modulus ratio of 1 indicating a purely elastic response, a value of 0 indicating a fluid-like response, and an intermediate value characterizing the range of viscoelastic responses between.

Shear modulus values were then corrected from a simplified assumption of incompressibility to values based on the compressibility of the indented tissue. A Poisson's ratio of 0.3, commonly assumed for cortical bone (Turner, Rho et al. 1999; Shahar, Zaslansky et al. 2007), was used for all zones; the accepted range of Poisson's ratio for cortical bone is generally between 0.28 and 0.33. Additionally, nanoindentation with atomic force microscopy on rabbit jaw fibrocartilage resulted in Young's moduli ranging from 0.95 to 2.34 MPa and Poisson's ratio between 0.30–0.46 (Hu, Radhakrishnan et al. 2001). Hence, using a constant value of 0.3 for all zones studied is a reasonable approximation. The shear modulus computed from the assumption of incompressibility (G^I) was converted to the shear modulus with a known constant but compressible ($\nu \neq 0.5$) Poisson's ratio (G^ν) by (Oyen 2007);

$$G^\nu = 2G^I(1-\nu) \tag{9}$$

The shear moduli were then converted to elastic moduli using

$$E = 2G(1+\nu) \tag{10}$$

The displacement-time curve fits resulting in R^2 values less than 0.999 or curve fits unable to capture the non-linear increase in displacement in the first 10 seconds of the hold segment were rejected (approximately 15% of the curves were rejected).

Statistical Analysis

Regression analysis was used to determine the relationship between elastic modulus and indent location. Each sample elastic modulus versus indent coordinate plot was split up into two sections; above and below the tidemark. A linear regression line was fit to each section and the slope was determined. A two factor (attachment [medial anterior attachment or medial posterior attachment], depth) analysis of variance (ANOVA) was performed using Minitab (Minitab 15 Statistical Software, State College, PA) to make comparisons between indents above and below the defined transition as well as between attachments. When significant results were identified by ANOVA, post-hoc comparisons were made using Tukey's method ($p<0.05$). Averages and standard deviations were calculated using the three tested samples for both depth and attachment. This analysis allowed for comparisons between the three anterior attachments tested and the three posterior attachments tested, without blocking by subject.

RESULTS

Displacements into the surface were the greatest for indentations nearest the external attachment and were much smaller in the subchondral bone (Figure 3a). A gradual increase in displacement into the surface as the indents move from subchondral bone towards the external attachment was evident (Figure 3a). Normalizing the response to the displacement after t_{rise} results in a broad spread of curves, suggesting that the time dependent response of creep does

not follow any given trend through the transition zones (Figure 3b). As expected though, the least amount of creep occurred in the subchondral bone and the most creep occurred in the uncalcified fibrocartilage.

The instantaneous elastic modulus values of each indent, as calculated from equation (9), can be seen in Figure 4. The instantaneous elastic modulus increased as the indentations progress from the ligamentous zone to the subchondral bone zone. The transition of stiffness through the insertion zones can be modeled bi-linearly. The modulus above the tidemark (nearest to the external ligament) changed less drastically with depth than that below the tidemark. This was quantitatively shown by determining the slope of the elastic modulus versus indent coordinate plots. The average slope above the tidemark (uncalcified fibrocartilage) for the instantaneous elastic modulus (1698±387 MPa/mm) was statistically lower than below the transition (calcified fibrocartilage and subchondral bone) (8929±3004 MPa/mm, $p=0.0130$). Also, the average slope of the infinite elastic modulus above the tidemark (2586±2611 MPa/mm) was found to be statistically lower than below the tidemark (5657±2060 MPa/mm, $p=0.0089$).

When paired by sample, the anterior attachment insertions were found to be stiffer than the posterior attachment insertions (Figure 5). For example, for an indentation coordinate of 0.0 mm (at the tidemark), the infinite time elastic modulus of the anterior insertion was 81% stiffer than the posterior insertion for one knee (sample A), and at an indentation coordinate of 0.05 mm (just deep to the tidemark), the instantaneous and infinite time elastic modulus of the anterior insertion of another knee (sample B) was 8% and 13% stiffer than the posterior insertion, respectively.

The instantaneous elastic moduli for the deepest indentation coordinates of each sample were found to be 24–51% larger than the infinite time elastic moduli. On average the infinite time elastic modulus to instantaneous elastic modulus ratio was 0.6 over all zones that were indented (Figure 6). The values were similar for both anterior and posterior attachments.

DISCUSSION

The insertional zones of interest in the meniscal attachment were the uncalcified fibrocartilage, calcified fibrocartilage, and subchondral bone. The uncalcified fibrocartilage zone is unmineralized, while the calcified fibrocartilage and subchondral bone zones are mineralized as they contain calcium. The nanoindentation technique presented here shows the ability of such a method to determine properties at the nano- to micro-scale, leading to knowledge of the local behavior of the meniscal attachment insertion sites. In this study, correlation of the individual indentation locations to each transition zone was not possible due to the inability to identify the interdigitations between the subchondral bone and the calcified fibrocartilage, however, a monotonic increase of elastic modulus across the zones was observed.

Determination of the elastic modulus gradient was limited by the approach to convert shear modulus values to elastic modulus values. Equation (10) assumes isotropic and homogeneous materials, however, subchondral bone is locally anisotropic. As such the values obtained here represent a functional stiffness, and one which derives from the anisotropic stiffness tensor and its relation to the indentation direction (Swadener, Rho et al. 2001).

A second limitation in performing mechanical tests on biological tissue is associated with hydration state. In the present study no steps were taken to dehydrate the sample prior to testing, as other nanoindentation studies of bone have done to eliminate the influence of changing environmental conditions (Rho, Roy et al. 1999; Bushby, Ferguson et al. 2004; Wang, Chen et al. 2006). Dehydration of samples removes the water contained within the tissue. While some have dehydrated their samples to permit true embedding using an infiltrating material

(Ferguson, Bushby et al. 2003), others do not embed the dehydrated samples. The polymer (e.g., PMMA) used for embedding can fill in the water space and, as such, the tissue may act in a manner that is very different to that of a dehydrated and non-embedded tissue. For example, cortical bone dehydrated in ethanol had a modulus of 15±2.2 GPa whereas PMMA embedded cortical bone was shown to have a modulus of 19.4 ± 2.1 GPa (Bushby, Ferguson et al. 2004). No explicit hydration system was used in the current study, and as such the results of this study should be taken as a guide for the stiffness trends in the transition from meniscal attachment to subchondral bone and not as absolute values of mechanical properties in a fully hydrated state.

Meniscal attachments have been characterized as tissues providing a gradual transition from the meniscus body to the bone of the tibial plateau. The circumferential tensile modulus of the meniscus body has been determined to be in the range of 43–150 MPa (Tissakht and Ahmed 1995; Lechner, Hull et al. 2000). The mean linear modulus of the human meniscal attachments (external ligamentous portion) of the meniscus region (ME), mid-substance region (MI), and bony insertion (BO) were found to be 153 ± 123 MPa, 195 ± 121 MPa, and 69.7 ± 33.7 MPa, respectively (Hauch 2008). The elastic modulus of cortical bone has been studied through nanoindentation and has been found to range from 20–27 GPa (Rho, Tsui et al. 1997; Turner, Rho et al. 1999; Bayraktar, Morgan et al. 2004). The modulus of the meniscal body and external attachments are in the same range and are both obtained from tensile tests. While the results from the current study may not provide absolute values for moduli in the different zones, the data shows a functional gradient exists as the tissue transitions from meniscus to bone. The current nanoindentation tests show that near the ligamentous zone of the attachment insertion, the elastic modulus was found to be in a similar range of the external meniscal attachments (tens of MPa). As the indentations moved into positive y-coordinates the elastic modulus increased substantially, reaching values as high as 4.3 GPa, believed to be in the deep regions of the subchondral bone. These results show that the insertional zones of the meniscal attachments serve as a transition from the relatively compliant meniscal attachments to the much stiffer cortical bone of the tibia. Again, tt is important to note that the values available for meniscal attachments are from tensile tests, not indentation. While the elastic modulus of cortical bone has been studied through nanoindentation and was found to range from 20–27 GPa (Rho, Tsui et al. 1997; Turner, Rho et al. 1999; Bayraktar, Morgan et al. 2004), specific studies on tibial subchondral bone showed a modulus of only 1.15GPa (Choi, Kuhn et al. 1990). Hence, in the current study on meniscal tibial insertions into subchondral bone values of 2GPa for modulus compare well with other published studies for similar tissue (Choi, Kuhn et al. 1990; Bembey, Bushby et al. 2006).

The insertion of the anterior cruciate ligament (ACL) to the subchondral bone has also been shown to transition through zones similar to the meniscal attachments. Using ultrasound elastographic imagining the insertion of the ACL was shown to involve complex strains with both compressive and tensile components occurring at the tibial insertion, with higher strains found at the insertion sites (Spalazzi, Gallina et al. 2006). More recently the compressive mechanical properties of the ACL-to-bone insertion have been documented using digital image correlation (Moffat, Sun et al. 2008). It has been shown using energy dispersive x-ray analysis that there is a regional mineral gradient across the fibrocartilage insertion zones which corresponds to the depth-dependent variations in compressive mechanical properties (Moffat, Sun et al. 2008). Additionally, these authors showed an increase in the apparent Young's modulus from unmineralized to mineralized fibrocartilage (unmineralized ~0.1 MPa, mineralized ~ 0.8 MPa). These modulus values are very different from those reported in the current study for both instantaneous and infinite modulus. This is likely due to the different techniques to obtain properties. The trends are similar however and indicate a gradual transition between zones at the insertion sites for both the ACL and meniscal attachments.

Evans et al,1990 has suggested that the amount of uncalcified fibrocartilage at the insertion of tendons and ligaments may be dependent on maximum force the tissue is exposed too, absolute size of the tendon or ligament, or the angle between the long axis of the tendon or ligament and the bone during joint movements (Evans, Benjamin et al. 1990). The authors show that the attachment site of the quadriceps tendon has a thickness for the uncalcified cartilage of 0.83mm on average, whereas for the origin and insertion of the patellar ligament is between 0.30 and 0.47 mm on average. In a follow-up study, these same authors studied the proportion of calcified tissue at the insertion of the quadriceps tendon and patellar ligament. Again, the quadriceps tendon was slightly thicker at 0.32mm and the patellar ligament was 0.2mm for the calcified tissue including both calcified cartilage and subchondral bone (Evans, Benjamin et al. 1991). The thickness of calcified fibrocartilage in the attachment zones of the medical collateral ligament, anterior cruciate ligament, posterior cruciate ligament and patellar ligament has previously been shown to be between 0.21 and 0.38mm (Gao and Messner 1996). Others have studied the insertion of the articular cartilage, meniscus and tendons and shown insertion zone thicknesses around 0.3–0.4mm (Benjamin, Evans et al. 1991; Benjamin, Toumi et al. 2006; Moffat, Sun et al. 2008). Therefore, it appears that many tissues, including the zones in the current study transition from one tissue type to another over an approximate range of 0.3mm.

Knowledge of the transition from the meniscal attachment into the bone is important to understand how this interface functions. Previous work on bone-cartilage interfaces determined mineral content at indentation locations in order to correlate moduli and mineral content. The elastic modulus gradually increased from the superficial zones of articular cartilage to the deeper calcified zones of subchondral bone (Tomkoria, Patel et al. 2004; Gupta, Schratter et al. 2005). Young's modulus in one study ranged from 0.52–1.69 MPa (Tomkoria, Patel et al. 2004) for rabbit tissue, while the other study showed much larger values of ~6–16 GPa (Gupta, Schratter et al. 2005) for human tissue. The increases in the measured modulus values correlated with increases in mineral content. Gupta et al., 2005 did not measure the unmineralized tissue, and dehydrated the samples which likely resulted in an elevated stiffness. Furthermore, Gupta et al., 2005 report reduced indentation modulus which includes both tip and sample stiffness, rather than assuming a Poisson's ratio as data presented in this study. Young's modulus through the various zones of insertion in the current study are on the order of Mpa's which more closely aligns with the data from Tomkoria et al. 2004. Samples in the current study were not dehydrated prior to embedding.

Previous nanoindentation studies showed that the largest changes in mechanical properties occurred across the interface between the unmineralized and mineralized cartilage, with very little change seen between the adjacent mineralized cartilage and subchondral bone (Ferguson, Bushby et al. 2003; Gupta, Schratter et al. 2005). Ferguson et al., 2003 reported values of roughly 19 GPa for dehydrated articular calcified cartilage and subchondral bone from human femoral heads. The indentation modulus dropped to approximately 14 GPa in the unmineralized cartilage, with a step in moduli values occurring at the tidemark. It is important to note that this tissue was embedded in PMMA which may have infiltrated the void spaces left in the tissue when the sample was dehydrated. Hence, the large values are likely due to the stiffening effects of the PMMA. The current data tends to show a more gradual increase in stiffness through all zones, albeit more dramatic in the mineralized tissue.

The maximum shear modulus values occurred at locations furthest from the tidemark in the subchondral bone and at instantaneous time. As an example, the instantaneous shear modulus of the medial posterior attachment of Sample C at a location 0.3 mm below the transition line was approximately 600 MPa, while the shear modulus at infinite time was approximately 450 MPa at the same location. This is consistent with the findings of Bembey et al. (2006) in which the instantaneous and infinite time shear moduli of equine cortical bone, tested in 0.9% saline,

were found to be 690 MPa and 490 MPa, respectively(Bembey, Bushby et al. 2006). This decrease in shear modulus over time shows the time dependence of the material. The present study shows comparable values for shear moduli.

This gradient of increasing stiffness through the insertion zones may serve the function of lessening the drastic change in properties between two different tissues to reduce the occurrence of failure at the interface. The instantaneous elastic modulus was found to be greater than the elastic modulus at infinite time indicating time dependence of the mechanical properties of even the nanostructure of the attachment insertions. It was also found that the zones of the anterior insertion sites possessed greater moduli than that of the matched posterior insertion sites. This finding is consistent with the linear modulus of the external anterior attachments being greater than the external posterior attachments possibly because the anterior attachments have been shown to be more mobile during loading. These data may be helpful in both computational modeling of meniscal attachments in whole knee joint models, as well as in the development of successful meniscal replacements.

Acknowledgments

This work is supported by the National Institutes of Health, (AR051906-01).

Nomenclature

h
: Displacement

t
: Time

B_0
: B_1, B_2, Exponential decay curve-fitting coefficients

τ_1
: τ_2, Time constants

C_0
: C_1, C_2, Creep compliance coefficients

P_{max}
: Fixed peak load

F_G
: Tip geometrical factor

$RCF_{1,2}$
: Ramp correction factor using τ_1 and τ_2 respectively

t_{rise}
: Rise time

R
: Indenter tip radius

G_0
: Instantaneous shear modulus

G_∞
: Infinite time shear modulus

ν	Poisson's ratio
G^I	Shear modulus computed from incompressibility assumption
G^ν	Corrected shear modulus based on an assumed Poisson's ratio
E	Elastic modulus
G	Shear modulus
$J(t)$	Creep Function

References

Alhalki MM, Howell SM, et al. How Three Methods for Fixing a Medial Meniscal Autograft Affect Tibia Contact Mechanics. The American Journal of Sports Medicine 1999;27(3):320–328. [PubMed: 10352767]

Bayraktar HH, Morgan EF, et al. Comparison of the elastic and yield properties of human femoral trabecular and cortical bone tissue. Journal of Biomechanics 2004;37:27–35. [PubMed: 14672565]

Bembey AK, Bushby AJ, et al. Hydration effects on the micro-mechanical properties of bone. Journal of Materials Research 2006;21(8):1962–1968.

Bembey AK, Bushby AJ, et al. Hydration effects on the micro-mechanical properties of bone. Journal of Materials Research 2006;21(8):1962–8.

Benjamin M, Evans EJ, et al. Quantitative differences in the histology of the attachment zones of the meniscal horns in the knee joint of man. J Anat 1991;177:127–34. [PubMed: 1769887]

Benjamin M, Evans EJ, et al. Quantitative differences in the histology of the attachment zones of the meniscal horns in the knee joint of Man. Journal of Anatomy 1991;177:127–134. [PubMed: 1769887]

Benjamin M, Toumi H, et al. Where tendons and ligaments meet bone: attachment sites ('entheses') in relation to exercise and/or mechanical load. J Anat 2006;208(4):471–90. [PubMed: 16637873]

Bushby AJ, Ferguson VL, et al. Nanoindentation of bone: Comparison of specimens tested in liquid and embedded in polymethylmethacrylate. Journa of Materials Research 2004;19(1):249–59.

Bushby AJ, Ferguson VL, et al. Nanoindentation of bone: Comparison of specimens tested in liquid and embedded in polymethylmethacrylate. Journal of Materials Research 2004;19(1):249–259.

Chen MI, Branch TP, et al. Is It Important to Secure the Horns During Lateral Meniscal Transplantation? A Cadaveric Study. The Journal of Arthroscopic and Related Surgery 1996;12(2):174–181.

Choi K, Kuhn JL, et al. The elastic moduli of human subchondral, trabecular, and cortical bone tissue and the size-dependency of cortical bone modulus. J Biomech 1990;23(11):1103–13. [PubMed: 2277045]

Cole BJ, Carter TR, et al. Allograft Meniscal Transplantation: Background, Techniques, and Results. The Journal of Bone and Joint Surgery 2002;84-A(7):1236–1250.

Constantinides G, Ravi Chandran KS, et al. Grid indentation analysis of composite microstructure and mechanics: Principles and validation. Materials Science and Engineering A 2006;430:189–202.

Cooper RR, Misol S. Tendon and Ligament Insertion. The Journal of Bone and Joint Surgery 1970;52-A(1):1–20. [PubMed: 4189231]

Donnelly E, Baker SP, et al. Effects of surface roughness and maximum load on the mechanical properties of cancellous bone measured by nanoindentation. Journal of Biomedical Materials Research 2006;77 (2):426–435. [PubMed: 16392128]

Ebenstein DM, Pruitt LA. Nanoindentation of soft hydrated materials for application to vascular tissues. Journal of Biomedical Engineering 2004;69A:222–232.

Evans EJ, Benjamin M, et al. Fibrocartilage in the attachment zones of the quadriceps tendon and patellar ligament of man. J Anat 1990;171:155–62. [PubMed: 2081702]

Evans EJ, Benjamin M, et al. Variations in the amount of calcified tissue at the attachments of the quadriceps tendon and patellar ligament in man. J Anat 1991;174:145–51. [PubMed: 2032930]

Ferguson VL, Bushby AJ, et al. Nanomechanical properties and mineral concentration in articular calcified cartilage and subchondral bone. J Anat 2003;203(2):191–202. [PubMed: 12924819]

Ferguson VL, Bushby AJ, et al. Nanomechanical properties and mineral concentration in articular calcified cartilage and subchondral bone. Journal of Anatomy 2003;203:191–202. [PubMed: 12924819]

Gao J. Immunolocalization of types I, II, and X collagen in the tibial insertion sites of the medial meniscus. Knee Surgery, Sports Traumatology, Arthroscopy 2000;8:61–65.

Gao J, Messner K. Quantitative comparison of soft tissue-bone interface at chondral ligament insertions in the rabbit knee joint. J Anat 1996;188 (Pt 2):367–73. [PubMed: 8621336]

Gao J, Oqvist G, et al. The attachments of the rabbit medial meniscus. A morphological investigation using image analysis and immunohistochemistry. Journal of Anatomy 1994;185:663–667. [PubMed: 7649801]

Gao J, Rasanen T, et al. The morphology of ligament insertions after failure at low strain velocity: an evaluation of ligament entheses in the rabbit knee. Journal of Anatomy 1996;189:127–133. [PubMed: 8771403]

Goertzen D, Gillquist J, et al. Tensile strength of the tibial meniscal attachments in the rabbit. Journal of Biomedical Materials Research 1996;30:125–128. [PubMed: 8788114]

Gupta HS, Schratter S, et al. Two different correlations between nanoindentation modulus and mineral content in the bone-cartilage interface. Journal of Structural Biology 2005;149:138–148. [PubMed: 15681230]

Hauch, KN. Time Dependent, Failure and Nanomechanical Properties of Meniscal Horn Attachments. Houghton: Michigan Technological University; 2008. Masters of Science

Hengsberger S, Kulik A, et al. A combined atomic force microscopy and nanoindentation technique to investigate the elastic properties of bone structural units. European Cells and Materials 2001;1:12–17. [PubMed: 14562266]

Hoffler CE, Guo XE, et al. An Application of Nanoindentation Technique to Measure Bone Tissue Lamellae Properties. Journal of Biomechanical Engineering 2005;127:1046–1053. [PubMed: 16502646]

Hu K, Radhakrishnan P, et al. Regional Structural and Viscoelastic Properties of Fibrocartilage upon Dynamic Nanoindentation of the Articular Cartilage. Journal of Structural Biology 2001;136:46–52. [PubMed: 11858706]

Hu K, Radhakrishnan P, et al. Regional structural and viscoelastic properties of fibrocartilage upon dynamic nanoindentation of the articular condyle. J Struct Biol 2001;136(1):46–52. [PubMed: 11858706]

Johnson, KL. Contact Mechanics. Cambridge, UK: Cambridge University Press; 1985.

Lechner K, Hull ML, et al. Is the Circumferential Tensile Modulus within a Human Medial Meniscus Affected by the Test Sample Location and Cross-Sectional Area? Journal of Orthopaedic Research 2000;18(6):945–951. [PubMed: 11192255]

Lee EH, Radok JRM. Contact problem for viscoelastic bodies. Journal of Applied Mechanics 1960;27:438–44.

Maes JA, Haut Donahue TL. Time dependent properties of bovine meniscal attachments: Stress relaxation and creep. Journal of Biomechanics 2006;39:3055–3061. [PubMed: 16360161]

Messner K, Gao J. The menisci of the knee joint. Anatomical and functional characteristics, and a rationale for clinical treatment (Review). Journal of Anatomy 1998;193:161–178. [PubMed: 9827632]

Moffat KL, Sun WH, et al. Characterization of the structure-function relationship at the ligament-to-bone interface. Proc Natl Acad Sci U S A 2008;105(23):7947–52. [PubMed: 18541916]

Oliver WC, Pharr GM. An improved technique for determining hardness and elastic modulus using load and displacement sensing indentation experiments. J Mater Res 1992;7(6):1564–1583.

Oyen ML. Spherical Indentation Creep Following Ramp Loading. Journal of Materials Research 2005;20:2094–2100.

Oyen ML. Nanoindentation hardness of mineralized tissues. Journal of Biomechanics 2006;39:2699–2702. [PubMed: 16253265]

Oyen ML. Sensitivity of polymer nanoindentation creep measurements to experimental variables. Acta Materialia. 2007

Oyen ML, Ko CC. Indentation Variability of Natural Nanocomposite Materials. Journal of Materials Research 2008;23:760–7.

Rho JY, Pharr GM. Effects of drying on the mechanical properties of bovine femur measured by nanoindentation. J Mater Sci Mater Med 1999;10(8):485–8. [PubMed: 15348117]

Rho JY, Pharr GM. Effects of drying on the mechanical properties of bovine femur measured by nanoindentation. Journal of Materials Science: Materials in Medicine 1999;10:485–488. [PubMed: 15348117]

Rho JY, Roy ME, et al. Elastic properties of microstructural components of human bone tissue as measured by nanoindentation. Journal of Biomedical Materials Research 1999;45:48–54. [PubMed: 10397957]

Rho JY, Tsui TY, et al. Elastic properties of human cortical and trabecular lamellar bone measured by nanoindentation. Biomaterials 1997;18(20):1325–1330. [PubMed: 9363331]

Setton LA, Guilak F, et al. Biomechanical Factors in Tissue Engineered Meniscal Repair. Clinical Orthopaedics and Related Research 1999;367S:S254–S272. [PubMed: 10546651]

Shahar R, Zaslansky P, et al. Anisotropic Poisson's ratio and compression modulus of cortical bone determined by speckle interferometry. Journal of Biomechanics 2007;40:252–264. [PubMed: 16563402]

Spalazzi JP, Gallina J, et al. Elastographic imaging of strain distribution in the anterior cruciate ligament and at the ligament-bone insertions. Journal of Orthopaedic Research. 2006(in press)

Swadener JG, Rho JY, et al. Effects of anisotropy on elastic moduli measured by nanoindentation in human tibial cortical bone. J Biomed Mater Res 2001;57(1):108–12. [PubMed: 11416856]

Tai K, Qi HJ, et al. Effect of mineral content on the nanoindentation properties and nanoscale deformation mechanisms of bovine tibial cortical bone. Journal of Materials Science: Materials in Medicine 2005;16:947–959. [PubMed: 16167103]

Tissakht M, Ahmed AM. Tensile stress-strain characteristics of the human meniscal material. Journal of Biomechanics 1995;28(4):411–422. [PubMed: 7738050]

Tomkoria S, Patel RV, et al. Heterogeneous nanomechanical properties of superficial and zonal regions of articular cartilage of the rabbit proximal radius condyle by atomic force microscopy. Medical Engineering and Physics 2004;26:815–822. [PubMed: 15567698]

Turner CH, Rho J, et al. The elastic properties of trabecular and cortical bone tissues are similar: results from two microscopic measurement techniques. Journal of Biomechanics 1999;32:437–441. [PubMed: 10213035]

Villegas DF, Hansen TA, et al. A Quantitative Study of the Microstructure and Biochemistry of the Medial Meniscal Horn Attachments. Annals of Biomedical Engineering 2008;36(1):123–131. [PubMed: 17999192]

Villegas DF, Maes JA, et al. Failure properties and strain distribution analysis of meniscal attachments. Journal of Biomechanics 2007;40(12):2655–2662. [PubMed: 17359982]

Wang XJ, Chen XB, et al. Elastic modulus and hardness of cortical and trabecular bovine bone measured by nanoindentation. Transactions of Nonferrous Metals Society of China 2006;16:s744–s748.

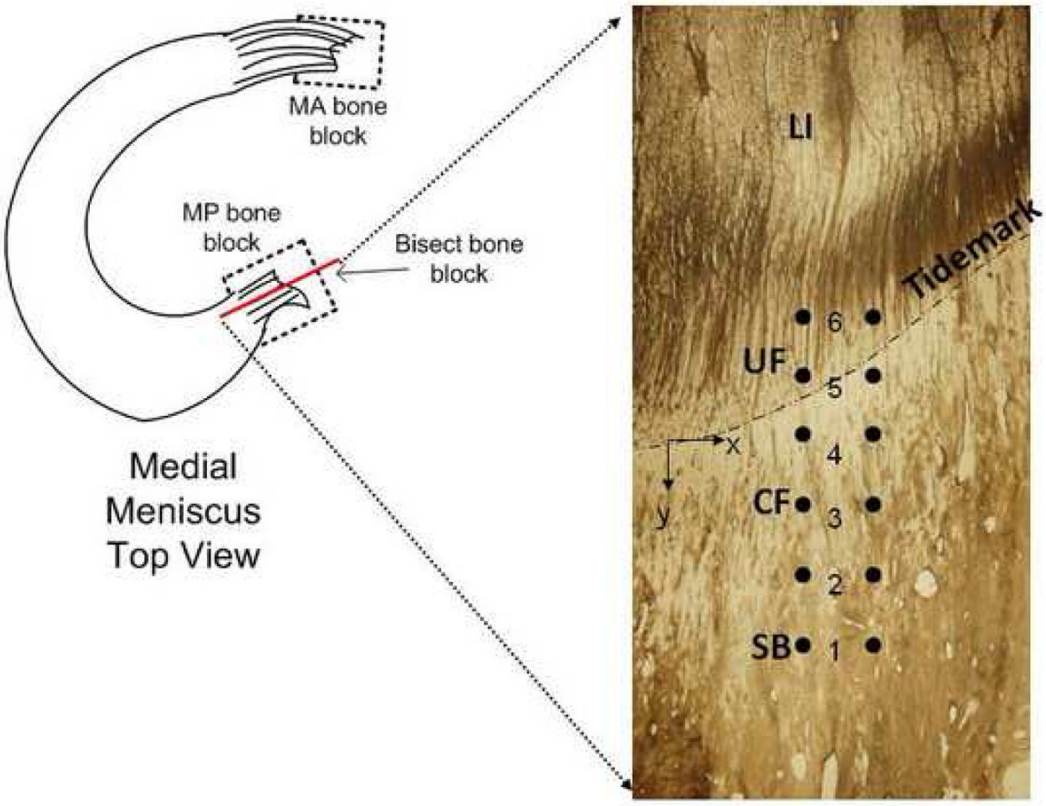

Figure 1.
Schematic of medial meniscus showing bone block locations and the indentation face of excised bone block (MA – medial anterior, MP – medial posterior) The transition zones of the attachment insertion (LI – ligamentous, UF – uncalcified fibrocartilage, CF – calcified fibrocartilage, SB – subchondral bone) are shown overlaid with markers of individual indentation locations. The tidemark is identified and is where y=0. Y is positive towards the subchondral bone.

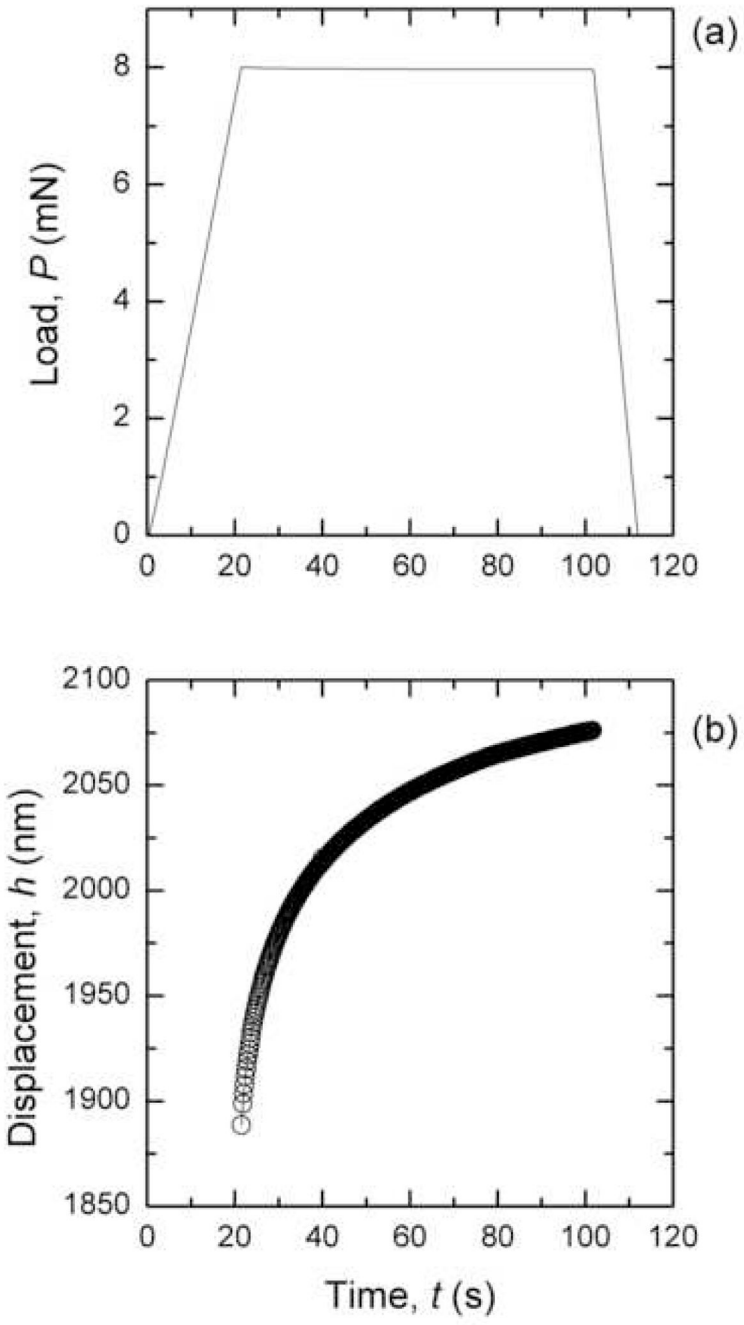

Figure 2.
a) Trapezoidal load-time sequence used in nanoindentation experiments, b) typical creep response during the peak load hold segment of nanoindentation experiments.

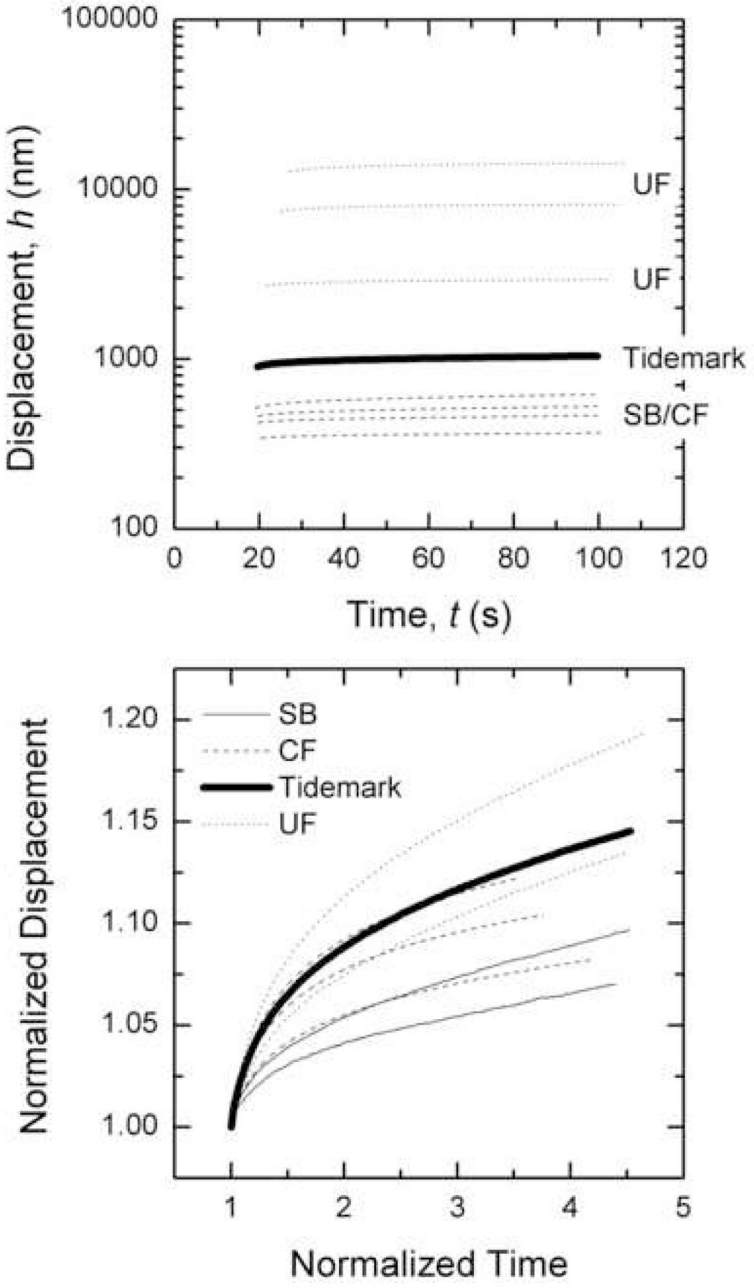

Figure 3.
Creep response during hold segment for 3 different regions; subchondral bone and calcified fibrocartilage (SB-CF), tidemark and uncalcified fibrocartilage (UF). b) Creep response normalized by the displacement and time at t_{rise}.

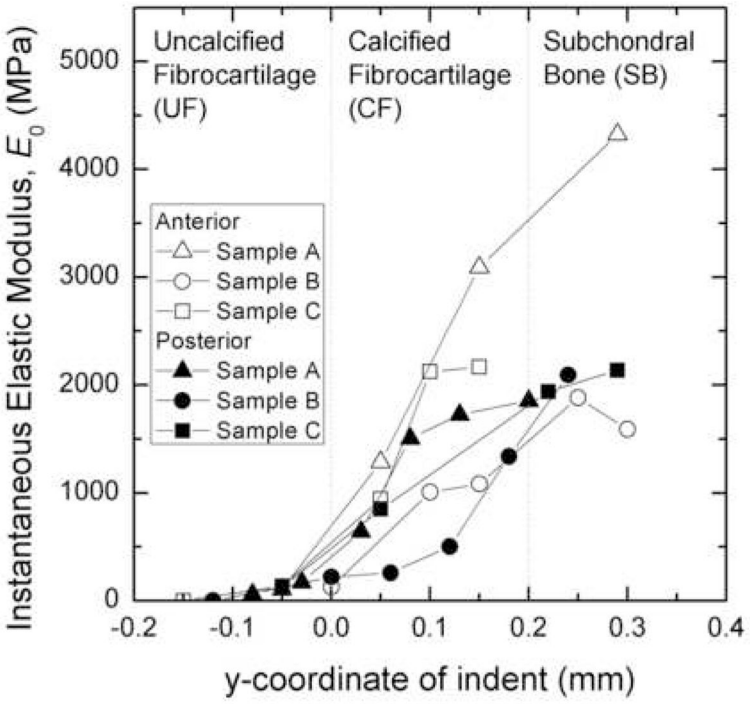

Figure 4.

Instantaneous elastic modulus as a function of indent location. A negative y coordinate corresponds to an indent located superior to the tidemark, while a positive y coordinate corresponds to an indent located distal to the tidemark in the mineralized tissue. The thickness of the zones was determined using data from human zone thicknesses determined by Benjamin et al. (1991) (Benjamin, Evans et al. 1991).

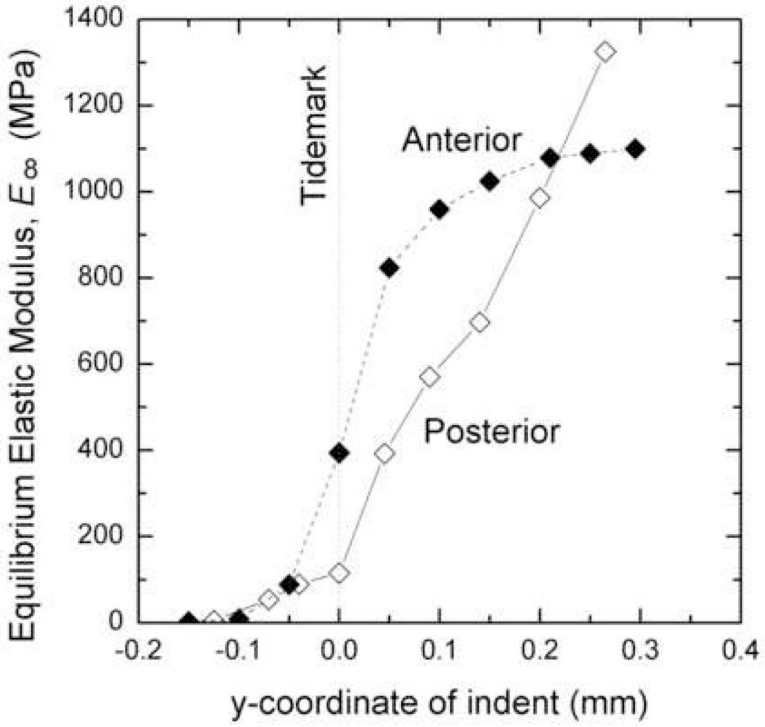

Figure 5.
Average elastic modulus at infinite time for anterior and posterior attachments. A negative y coordinate corresponds to an indent located above the tidemark while a positive y coordinate corresponds to an indent located below the tidemark.

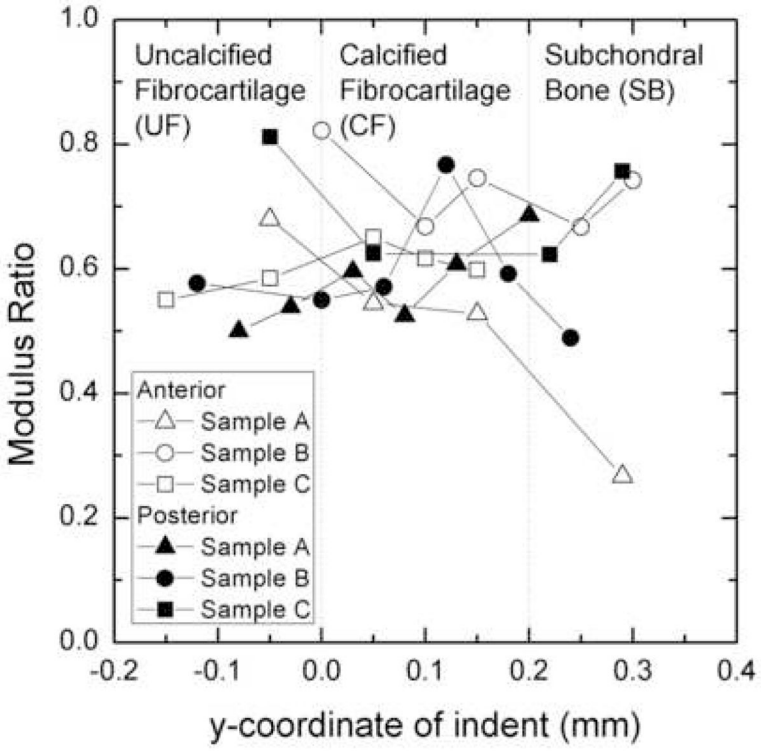

Figure 6.
Plot of the ratio of the infinite time elastic modulus to the instantaneous elastic modulus for various attachments tested. A negative y coordinate corresponds to an indent located above the tidemark while a positive y coordinate corresponds to an indent located below the tidemark.